The Effect of Postweld Heat Treatment on Hydrogen-Assisted Cracking of F22/625 Overlays

Hydrogen-assisted cracking at the interface of F22/Alloy 625 weld overlays is found to be a strong function of PWHT using the delayed hydrogen cracking test

T. DAI AND J. C. LIPPOLD

ABSTRACT

The weld interface of Alloy 625 clad on F22 (2.25Cr-1Mo) steel is known to be susceptible to hydrogen-assisted cracking (HAC) and sulfide stress cracking (SSC) following postweld heat treatment (PWHT). The PWHT is applied to meet an industry standard that requires a maximum heat-affected zone (HAZ) hardness below 250 VHN (~22 HRC). In this study, a range of PWHT conditions was evaluated to determine the actual susceptibility to HAC using the delayed hydrogen cracking test (DHCT). Based on this test, a range of PWHT conditions was identified using the Hollomon-Jaffe parameter (HJP), where resistance to HAC was optimized. The DHCT results and hardness testing combined revealed that the PWHT range (19,500 to 20,200) had optimum resistance to HAC. At lower HJP values, the HAZ hardness was above the industry standard, while at higher values carbon migration to the interface embrittled the planar growth zone (PGZ) in the weld metal. This embrittlement led to reduced failure times in the DHCT. Metallographic and fractographic examination of failed DHCT samples confirmed the location and nature of the failures.

KEYWORDS

- Postweld Heat Treatment • Hollomon-Jaffe Parameter
- F22/625 Dissimilar Weld Metal • Hydrogen-Assisted Cracking
- Delayed Hydrogen Cracking Test • Hardness • Fractography

Introduction

An Alloy 625 overlay on F22 steel is widely used for subsea oil platform components to provide corrosion protection. In some applications, the fusion boundary of F22/625 will be exposed to production fluid, making it potentially susceptible to sulfide stress cracking (SSC) if the overlay weld is not properly heat treated. Postweld heat treatment (PWHT) must be utilized to reduce the hardness in the heat-affected zone (HAZ), especially the coarse-grain HAZ (CGHAZ), to reduce its susceptibility to SSC. The National Association of Corrosion Engineers (NACE) standard MR0175 and the International Standards Organization (ISO) standard 15156 (Ref. 1) require that the maximum as-tempered hardness of the steel not exceed 22 HRC or 250 VHN.

It is well known that PWHT will promote carbon migration from the F22 steel to the fusion boundary, resulting in a "pile up" of carbon in a narrow region at the fusion boundary (Refs. 2–4). Specifically, the narrow region is the planar growth zone (PGZ), or "featureless" zone, which has been described in detail in a previous paper (Ref. 5). After PWHT, the high hardness in the PGZ was found to be the most susceptible to hydrogen-assisted cracking (HAC) (Refs. 6, 7). Thus, an optimum PWHT would reduce the CGHAZ hardness to meet the requirements of the standard while preventing interface embrittlement by hydrogen diffusion. Identifying this PWHT "sweet spot" was the motivation for a previous study of weld interface hardness under a wide range of PWHT conditions (Ref. 5).

There are different test methods that have been used to evaluate HAC in weld overlays. One is a simple bend test on a sample with a notch for stress concentration. These include the three-point bend test, or single-edge notch bend test (Refs. 6–8), and the four-point bend test (Ref. 9). For these tests, the hydrogen was pre-charged into the samples before bending (Refs. 6–9). For the F22/625 sample, the notch tip was machined exactly at the fusion boundary, and thus the fracture initiation was predetermined from the weld interface (Refs. 6, 7). A slow strain rate tensile test (Refs. 10–12) can also produce failure similar to the bend test. The dynamic strain of the bend test and the slow-strain rate tensile test is effective in producing sample failure, but it does not simulate the actual condition where the stress and/or strain in the sample does not change dynamically with time.

To evaluate the HAC of the weld interface, The Ohio State University developed the delayed hydrogen cracking test (DHCT), which has been shown to be an accelerated HAC test that is very sensitive to PWHT conditions (Refs. 13–15). The test uses constant load so the interface nominal stress remains constant before fracture initiation, and hydrogen is charged into the sample during the test, as would occur in practice. There are various choices of charg-

https://doi.org/10.29391/2018.97.007

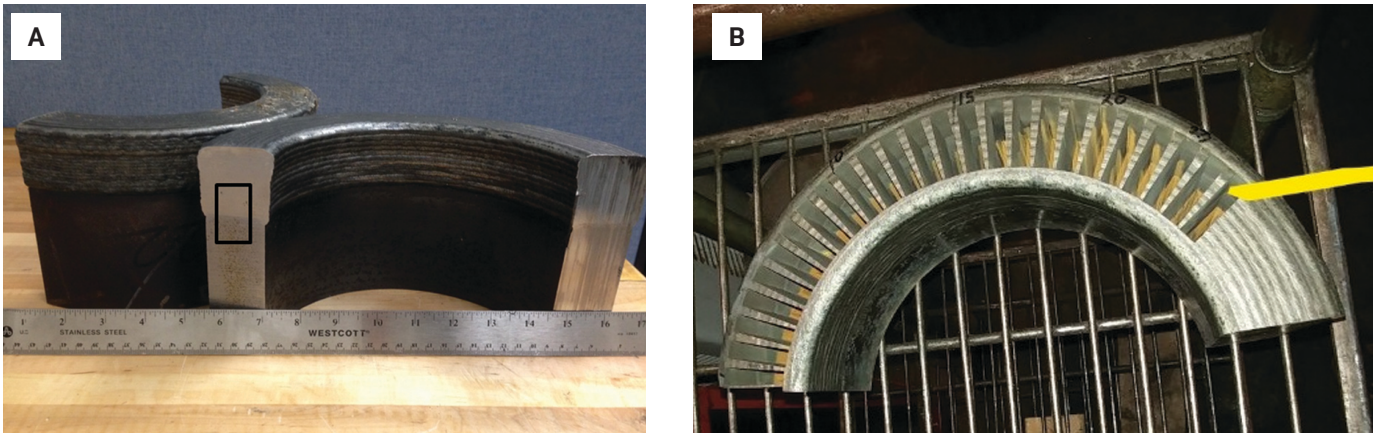

Fig. 1 — A — F22/625 dissimilar metal weld coupon; B — coupon after EDM machining of DHCT samples.

ing solutions and hydrogen recombination poisons (Ref. 16). Acidic charging solutions represent an oil-production fluid more closely than alkaline-charging solutions (Ref. 17). As_2O_3 (Ref. 8) is an effective and stable hydrogen recombination poison, but it's hazardous to human health and, therefore, not used in the present study.

In the DHCT work by Bourgeois (Ref. 15), the load was set to a certain constant percent of the yield strength of each sample (e.g., 90%, 70%, 50%, etc.). However, the F22/625 overlay interface had a range of yield strength as a function of PWHT. In this study, using a constant stress facilitated the comparison of the effect of the PWHT, and simulated the actual scenario in practice. The tensile stress cannot be too small for HAC, and must be above a threshold minimum value, as found by Yue (Ref. 18).

Fenske et al. (Ref. 19) studied three PWHT conditions on F22/625 welds: 649°C/5 h, 649°C/10 h, and 649°C/15 h. He found that the M_7C_3 carbides started to precipitate in the PGZ of the F22/625 overlay tempered at 649°C/15 h, but he did not relate HAC susceptibility to the PWHT conditions. Dodge (Ref. 6) studied the as-welded condition and three PWHT conditions on F22/625 welds: 650°C/1 h, 650°C/10 h, and 650°C/100 h. He observed that the fracture path was along the fusion boundary in the as-welded condition, but propagated through the PGZ in all the PWHT conditions. With the most severe PWHT condition (650°C/100 h), precipitation of M_7C_3 carbides in the PGZ was thought to be the reason for high HAC susceptibility (Ref. 6).

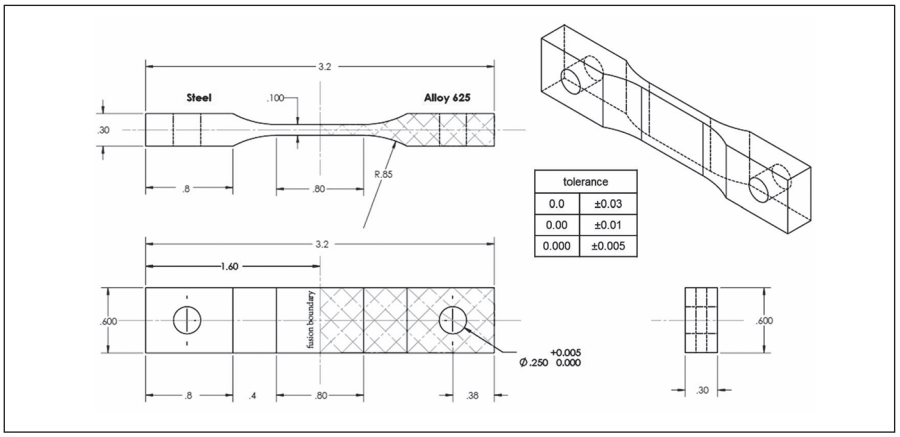

Fig. 2 — Sample geometry for the DHCT with units in inches.

In this study, 11 PWHT conditions were used to better understand its effect on HAC susceptibility. This wider PWHT range was selected to encompass the ones from the previous studies. Again, the motivation for this study was to determine the potential range of PWHT conditions that provide optimum resistance to HAC.

Table 1 — Welding Parameters Used for Overlay of Alloy 625 on F22 Steel Forging

Step Increment (in.)	Voltage (V)	Peak Current (A)	Background Current (A)	Hot Wire Voltage (V)	Wire Feed Speed (in./min)	Preheat Temperature (°C/°F)
0.150	11.0	240.0	120.0	3.3	66.9–82.2	176.7/350
Interpass Temperature (°C/°F)	**Travel Speed (in./min) (in./min)**	**Hot Wire Peak Current (A)**	**Hot Wire Background Current (A)**	**Heat Input (kJ/in.)**	**Deposition Rate (lb/h)**	**Shielding Gas Flow Rate (ft^3/h)**
287.8/550	7.9	179.0	55.0	10.0	2.0	30.0

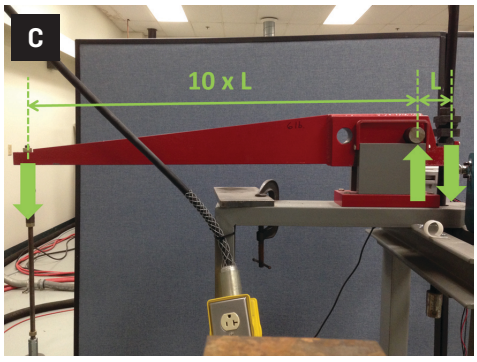

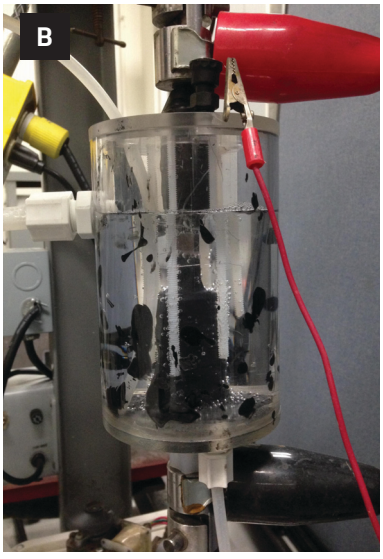

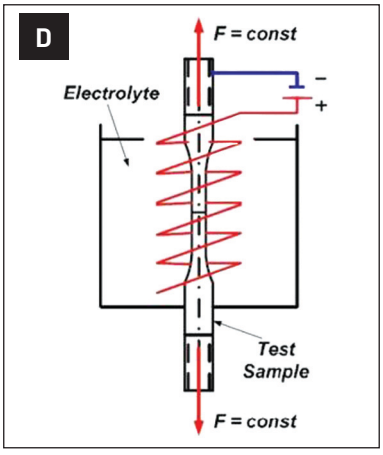

Fig. 3 — A — Overview of the DHCT system; B — loaded sample immersed in hydrogen-charging solution; C — loading lever; D — hydrogen-charging circuit. (Courtesy of D. Bourgeois.)

Experimental Procedures

Material

The F22 steel was in the form of a forged pipe 11.25 in. (286 mm) in diameter with a nominal 2.50-in. (63.5-mm) wall thickness. The weld overlay with Alloy 625 (ERNiCrMo-3) was performed using the hot-wire gas tungsten arc welding (HW-GTAW) process with the parameters listed in Table 1.

The overlay was clad on the surface of the pipe cross section as shown in Fig. 1A. The thickness of the overlay was approximately 1.7 in. (43.2 mm), which is thicker than what was used in practice to accommodate the machining of the DHCT samples that would allow the fusion boundary to be located in the gauge section.

Table 2 shows the compositions of the F22 steel base metal and Alloy 625. Table 3 provides the mechanical properties of the F22 steel base metal, the 625 welding wire, and the dissimilar weld metal in the as-welded condition.

Sample Preparation

Samples were cut from the F22/625 overlay coupon with electron discharge machining (EDM) (Fig. 1B), and machined to the DHCT geometry shown in Fig. 2. The delayed hydrogen cracking test samples were conducted under constant load in conjunction with a hydrogen-charging system. There is no standardized sample geometry for the DHCT, so a reduced gauge-section sample was used with the weld interface perpendicular to the loading direction and in the middle of the gauge section. The width of the sample was 0.6 in., which encompassed approximately four weld bead widths from the original overlay.

Postweld Heat Treatment Conditions

Eleven PWHT conditions were used to temper the machined samples (Table 4). For each condition, at least two specimens were tempered for repeatability. The degree of tempering during PWHT was represented by the Hollomon-Jaffe parameter (HJP), calculated from Equation 1 with the temperature (T) in kelvin and the time (t) in hours (Ref. 20). The first five PWHT conditions listed in Table 4 are commonly used in industry, and the latter six with larger HJP values were used to better understand extreme conditions of PWHT (e.g., 660°C/100 h). Because the HJP combines temperature and time, different combinations of the tempering temperature and tempering time can yield the same HJP. Two HJPs were selected

Table 2 — Chemical Composition of F22 Steel and Filler Metal Alloy 625

Wt.%	C	Ni	Cr	Mn	Si	Mo	S	P	Al	Cu	Ti	Nb	Fe
BM F22	0.15	0.11	2.28	0.60	0.30	0.98	0.009	0.009	0.022	0.12	0.001	0.002	bal.
FM 625	< 0.01	64.0	22.7	< 0.01	0.04	9.0	0.001	< 0.01	0.12	< 0.011	0.23	3.59	0.3

Table 3 — Mechanical Properties of F22, Alloy 625, and Dissimilar Overlay

	UTS/ksi	YS/ksi	% EL	% RA	Note
BM F22	98.85	79.55	26.6	76.8	Provided by Cameron
FM 625	114.0	85.0	—	—	Provided by Acute
F22/625 as-welded	98.12	64.33	12.78	58.33	Tested at OSU, failure in the BM

— HJP = 19,593 corresponding to 660°C/10 h and 640°C/28.84 h, as well as HJP = 19,874 corresponding to 660°C/10 h and 640°C/58.6 h (Table 4) — to study the effect of the same HJP with different PWHT conditions on the HAC behavior.

$$HJP = T * (20 + \log t) \quad (1)$$

The samples were tempered in argon using a horizontal tube furnace containing a titanium sponge to reduce oxidation. Type K thermocouples were used to verify that the samples reached furnace temperature in approximately 10 to 20 min. The heating time was not included in the total time for calculation of HJP. Samples were quenched in water at the completion of tempering.

Delayed Hydrogen Cracking Test

The delayed hydrogen cracking test (DHCT) is essentially a constant-load lever system (Fig. 3A and C) used to apply constant tensile stress on the loaded sample. A reservoir was used for the hydrogen-charging solution, which was circulated through a transparent plastic container where the sample was submerged and the charging current was applied (Fig. 3B). The charging solution was sulfuric acid (H_2SO_4) with pH = 1.29 ± 0.02 (10 L distilled water + 27.5 mL H_2SO_4, or 0.05145 mol/L) maintained at a temperature of 22 ± 2°C. Five grams of sodium thiosulfate ($Na_2S_2O_3$) was added to the solution as the hydrogen recombination poison. Each test started 24 h after making the fresh charging solution. Additional details of the DHCT procedure can be found elsewhere (Ref. 15).

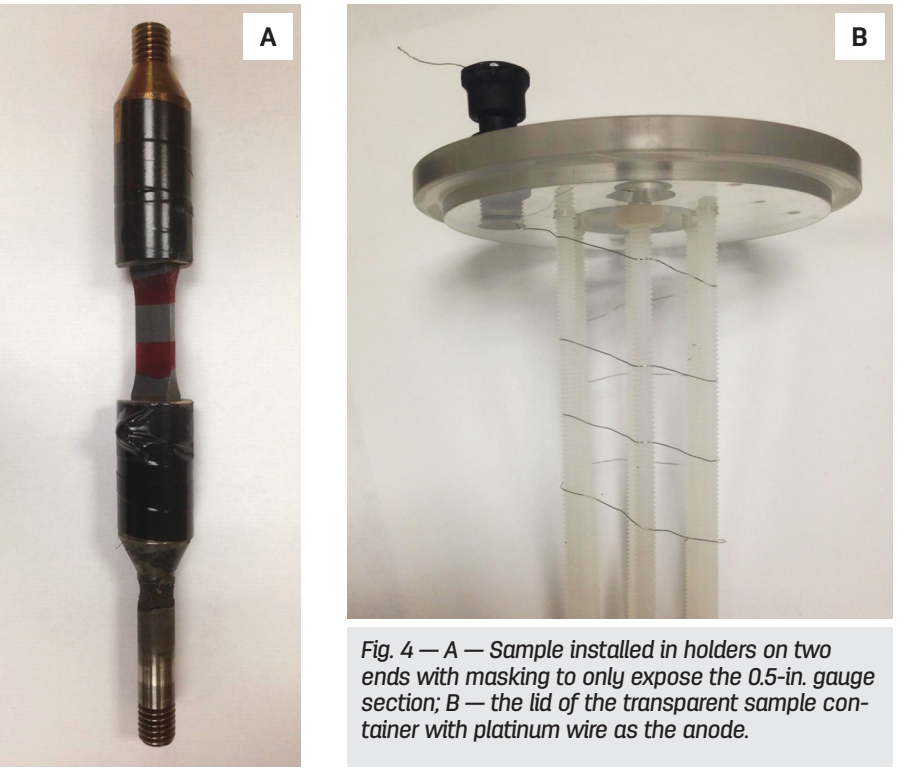

Fig. 4 — A — Sample installed in holders on two ends with masking to only expose the 0.5-in. gauge section; B — the lid of the transparent sample container with platinum wire as the anode.

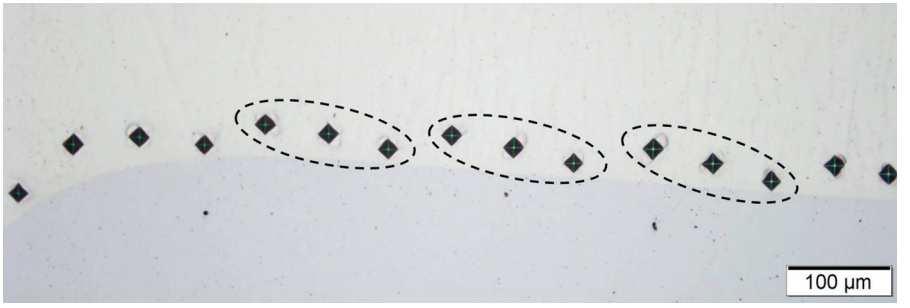

Fig. 5 — Microhardness indentations along the fusion boundary for obtaining the hardness in the PGZ.

A masking agent was applied to the gauge section so that only 0.5 in. (12.7 mm) of the gauge section was exposed to the charging solution. This exposed region represented approximately 0.125 in. of Alloy 625 and 0.375 in. of the F22 steel — Fig. 4A. This exposed region contained the weld metal, transition zone, and the entire F22 HAZ. Corrosion of the steel by sulfuric acid

Table 4 — PWHT Conditions of F22/625 Samples

Heat Treatment	Temperature	Time	HJP
HT-1	660°C or 1220°F	2 h	18,941
HT-2	640°C or 1184°F	6 h	18,970
HT-3	650°C or 1202°F	10 h	19,383
HT-4	660°C or 1220°F	10 h	19,593
HT-5	640°C or 1184°F	28.84 h	19,593
HT-6	660°C or 1220°F	20 h	19,874
HT-7	640°C or 1184°F	58.6 h	19,874
HT-8	660°C or 1220°F	50 h	20,154
HT-9	660°C or 1220°F	100 h	20,526
HT-10	660°C or 1220°F	240 h	20,881
HT-11	660°C or 1220°F	500 h	21,178

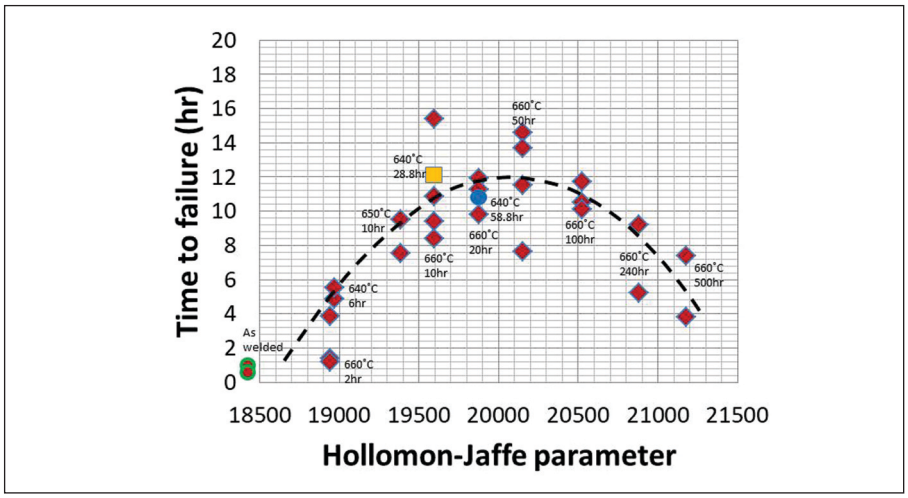

Fig. 6 — Summary of the DHCT results and the trend line of TTF with respect to the HJP.

and galvanic corrosion between the two alloys were inhibited because the sample was the cathode in the charging system and was cathodically protected. Positive hydrogen ions moved toward the sample (cathode) to obtain electrons to form hydrogen atoms or hydrogen gas. The anode was a platinum wire that surrounded the sample. Figure 4B shows the lid of the container and the platinum wire. Figure 3D shows the charging circuit.

A constant load was applied for all the F22/625 samples in different PWHT conditions. Through trial and error, a tensile stress of 61 ksi was used for all testing, which represents approximately 90% of the yield strength of the sample at a PWHT condition of 660°C/2 h (HJP = 18,941). Both sodium thiosulfate and thiourea were evaluated for use as the hydrogen recombination poison. Sodium thiosulfate was not as stable as thiourea in solution, but the effectiveness of the hydrogen recombination of thiourea was much less than sodium thiosulfate. Thus, sodium thiosulfate was used in the DHCT for this investigation.

Vickers Hardness Testing

Two sections removed from each sample gauge section were tempered together with their parent sample for the DHCT. A section containing the fusion boundary was cut and mounted in Bakelite to make a sample for hardness mapping and testing. The detail of the hardness testing procedure can be found elsewhere (Ref. 5). Indentations (100 g load) were made adjacent to the fusion boundary to obtain the average and maximum hardness in the PGZ. Every three indents were a set, as circled in Fig. 5. Three indents were needed due to the variation of distance be-

Table 5 — DHCT Results of F22/625 Samples in Different PWHT Conditions

# Sample	PWHT	HJP	TTF (h)	Initiation Location
1	As-welded	—	1.02	CGHAZ
2	As-welded	—	0.83	CGHAZ
3	660°C/2 h	18941	1.38	Fusion boundary
4	660°C/2 h	18941	3.85	Fusion boundary
5	660°C/2 h	18941	1.17	Fusion boundary
6	640°C/6 h	18970	4.87	Fusion boundary
7	640°C/6h	18970	5.5	Fusion boundary
8	650°C/10 h	19383	9.5	Fusion boundary
9	650°C/10 h	19383	7.53	Fusion boundary
10	660°C/10 h	19593	8.4	Fusion boundary
11	660°C/10 h	19593	10.87	Fusion boundary
12	660°C/10 h	19593	15.4	Fusion boundary
13	660°C/10 h	19593	9.4	Fusion boundary
14	640°C/28.84 h	19593	12.13	Fusion boundary
15	660°C/20 h	19874	9.8	PGZ
16	660°C/20 h	19874	11.9	PGZ
17	660°C/20 h	19874	11.28	PGZ
18	640°C/58.6 h	19874	10.82	PGZ
19	660°C/50 h	20154	14.6	PGZ
20	660°C/50 h	20154	7.63	PGZ
21	660°C/50 h	20154	13.7	PGZ
22	660°C/50 h	20154	11.53	PGZ
23	660°C/100 h	20526	11.7	PGZ or fusion boundary
24	660°C/100 h	20526	10.5	PGZ or fusion boundary
25	660°C/100 h	20526	10.1	fusion boundary
26	660°C/240 h	20881	9.2	fusion boundary
27	660°C/240 h	20881	5.2	fusion boundary
28	660°C/500 h	21178	3.82	fusion boundary
29	660°C/500 h	21178	7.37	fusion boundary

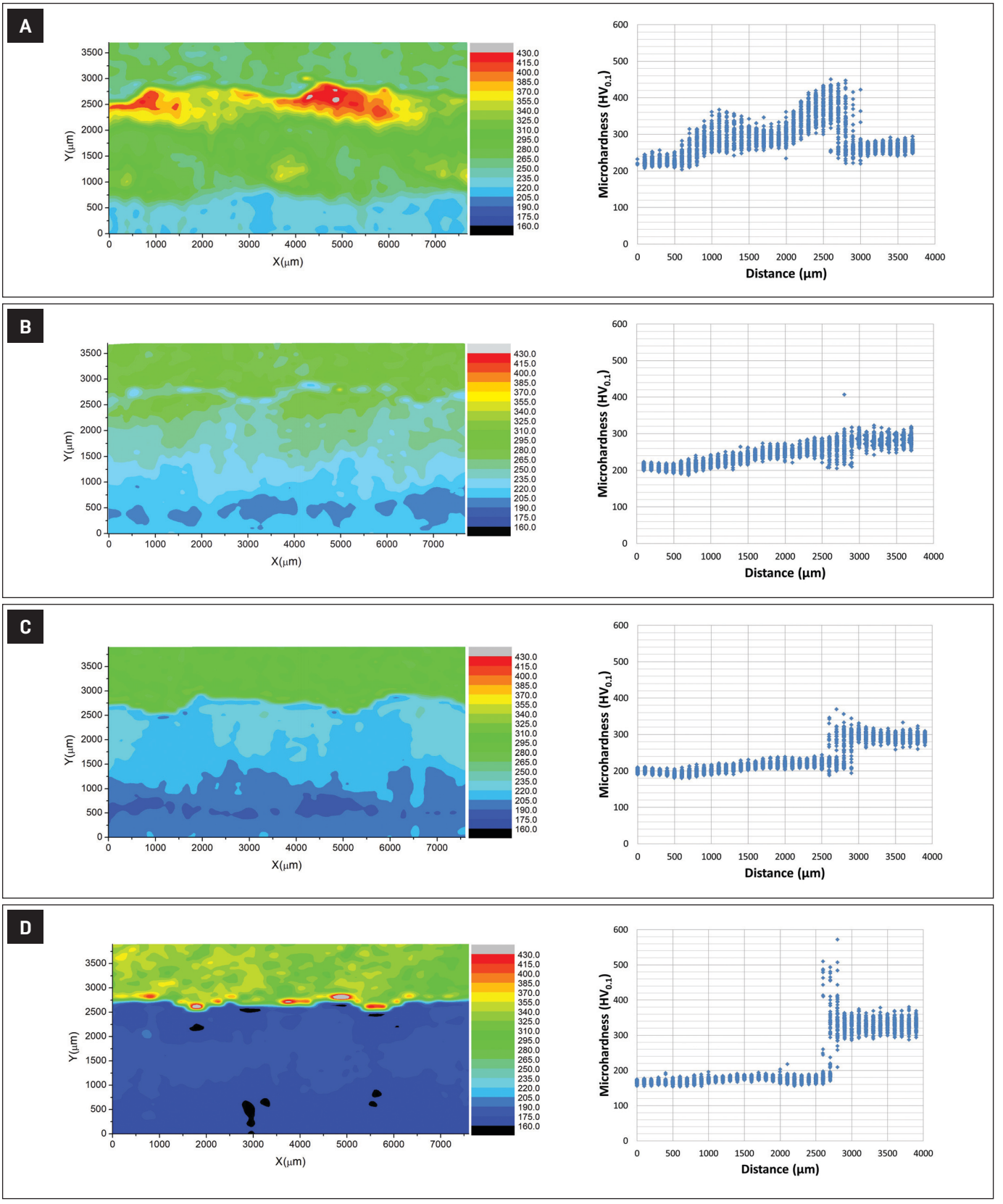

Fig. 7 — Hardness maps and hardness distributions of PWHT samples (Ref. 5): A — As-welded; B — 640°C/6 h; C — 660°C/20 h; D — 660°C/500 h.

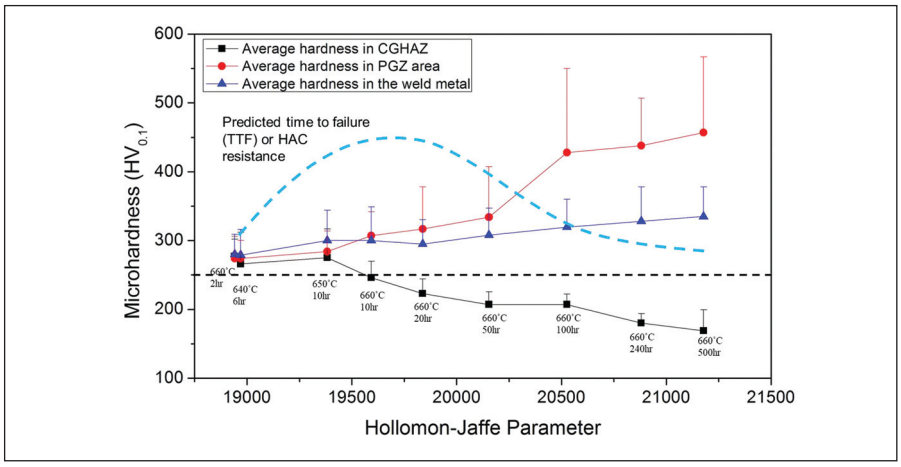

Fig. 8 — Summary of hardness response in the CGHAZ, WM, and PGZ areas as a function of the HJP, as well as the predicted TTF trend with the HJP according to hardness variation.

tween hardness peaks and the fusion boundary. The maximum hardness of each set was selected to obtain the average and maximum hardness adjacent to the fusion boundary.

Fractography and Identifying Crack Initiation Location

After failure, the sample was immediately removed from the DHCT charging solution, rinsed with water and ethanol, and hot-air dried. Both sides of the fractured sample were characterized with the scanning electron microscope (SEM [Quanta 200 or XL-30 ESEM]). Energy dispersive x-ray (EDX) analysis was also utilized to determine the composition of the fracture surface at the location of crack initiation. This information was used to determine the exact region of crack initiation without the need for sample sectioning. Estimates of the fracture initiation location were made using this method.

Results

Variation of Time to Failure with the Hollomon-Jaffe Parameter

The DHCT failure data in terms of time-to-failure (TTF) for the as-welded and different PWHT conditions are listed in Table 5. The TTF is plotted as a function of the HJP in Fig. 6. Generally, as the HJP increases, the TTF of the samples increases and then decreases after achieving a maximum value. HJP is a continuous value, and only nine discrete HJPs were tested using the DHCT. The as-welded samples failed at very short test times, at approximately 1 h. These failures occurred in the CGHAZ, which exhibited hardness levels in excess of 450 VHN. All the PWHT conditions exhibited longer TTF values relative to the as-welded condition, indicating an increase in the HAC resistance with heat treatment. The maximum TTF, representing the most resistant condition, was at 660°C/50 h. Taking data scatter into consideration and the trend line of TTF with regard to the HJP (Fig. 6), the "sweet spot" of PWHT for the maximum TTF was in the HJP range of 19,800 to 20,200.

It should be noted that the HJP appears to be a good indicator of TTF, irrespective of the PWHT temperature. This can be supported by two examples: HJP = 19,593 and HJP = 19,874. PWHT 660°C/10 h and 640°C/28.84 h had equal HJP = 19,593; the average TTF of PWHT 660°C/10 h was 11.02 h, only slightly lower than the TTF (640°C/ 28.84 h) = 12.13 h. Also, PWHT 660°C/ 20 h and 640°C/58.6 h had equal HJP = 19,874; the average TTF of PWHT 660°C/20 h was 11.0 h, very close to the TTF (640°C/58.6 h) = 10.82 h.

Hardness Evaluation of Samples Tested using DHCT

The fusion boundary region (CGHAZ, PGZ, and weld metal [WM]) in the as-welded and 11 PWHT conditions were evaluated using hardness mapping. Figure 7 shows the hardness maps and hardness distributions of the as-welded condition and selected samples at three PWHTs. Hardness maps for additional PWHT conditions and the fusion boundary microstructure have been published previously (Ref. 5). The hardness distribution plots associated with these maps can show the quantitative variation of hardness in the CGHAZ, PGZ, and WM. As the HJP increases, the CGHAZ hardness decreases due to tempering of the martensite, and WM hardness increases due to precipitation. Also, with increased tempering time and temperature, hardness peaks appear in the PGZ due to carbon diffusion and buildup — Fig. 7B to D.

The CGHAZ of the as-welded sample was not homogeneous due to the tempering effect of the multibead overlay where adjacent passes provided some tempering effect. In the as-welded condition, the CGHAZ hardness of up to 450 $HV_{0.1}$ was observed (in the hardness scale bars of Fig. 7, gray color scale is > 430 $HV_{0.1}$ and the black color scale is < 160 $HV_{0.1}$). The PWHT at 640°C/6 h decreased the average CGHAZ hardness to 270 $HV_{0.1}$, while PWHT at 660°C/20 h reduced the average CGHAZ hardness to 220 $HV_{0.1}$. In both cases, there was no strong hardness peak observed in the PGZ. Hardness values up to 500 $HV_{0.1}$ were present at the fusion boundary after PWHT at 660°C/500 h.

The average and maximum hardness of the CGHAZ, PGZ, and WM are summarized in Fig. 8. If only the effect of hardness on HAC susceptibility is considered, the variation of TTF (HAC resistance) with respect to the HJP is approximated by the blue dashed curve in Fig. 8. The blue dashed curve is only a predicted trend of TTF, based on which the optimal HJP range can be inferred as ~19,500 to 19,800.

Fracture Morphology after DHCT

Eight samples were selected to show the morphology of the fracture surface. Only the fracture surface on the Alloy 625 side of the sample was shown because the corresponding fracture surface on the F22 steel side is a "mirror-image." The black lines on the macroscopic fracture surfaces shown in Fig. 9 separate regions with different fracture

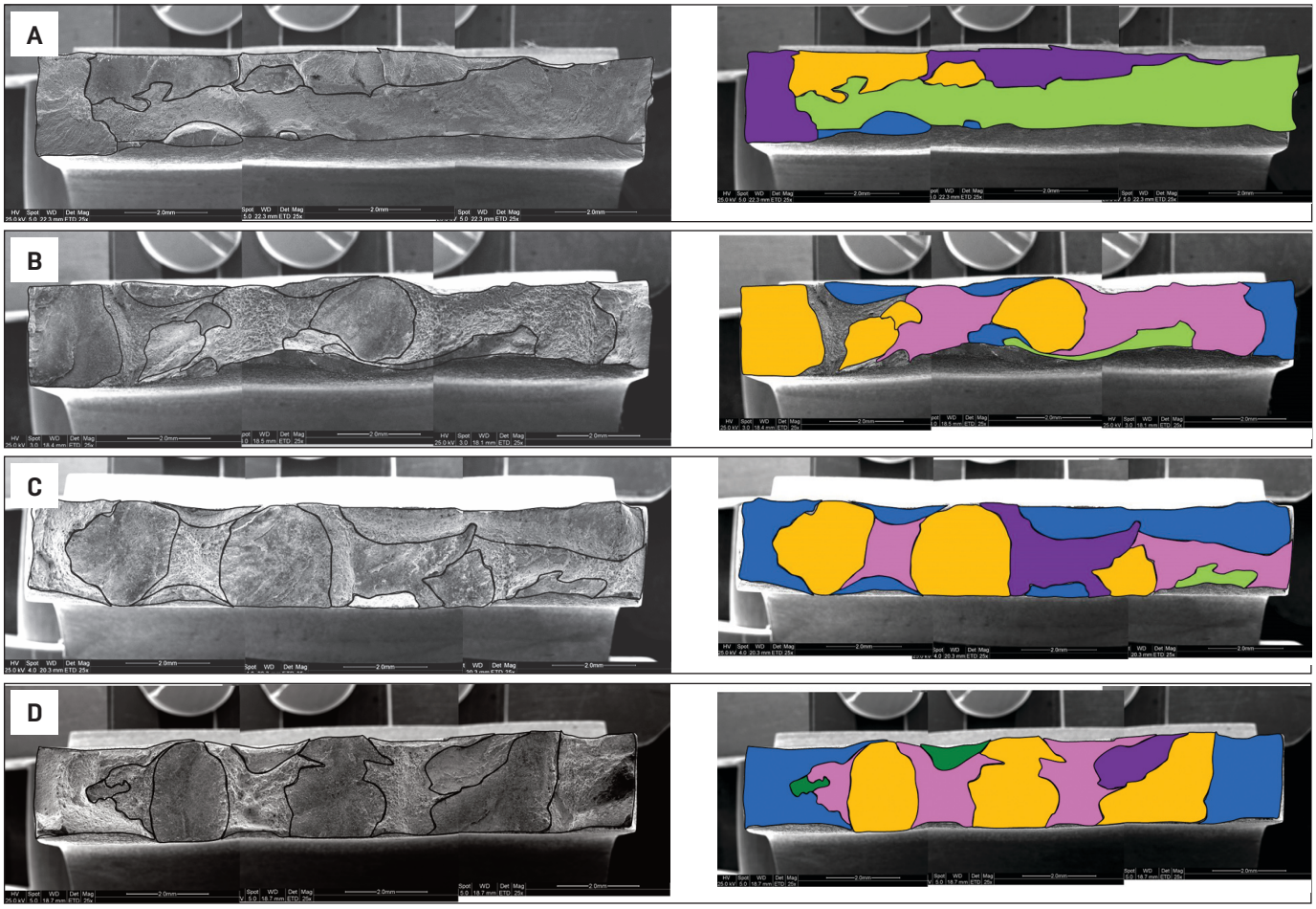

Fig. 9 — The fracture surface of different samples on the Ni-alloy 625 side and the different typical morphologies are represented by different colors: A — As-welded; B — 640˚C/6 h; C — 660˚C/10 h; D — 660˚C/20; Light green = microvoid coalescence in weld metal by overload; purple = quasi-cleavage in the CGHAZ; orange = fusion boundary fracture; pink = microvoid coalescence in the base metal; dark green = quasi-cleavage, cleavage, or terrace fracture in the PGZ; blue = overload fracture in the base metal.

morphologies. These fracture morphologies were then color-coded to show the relative proportions. Each of these fracture morphologies with distinguishing colors will be described in the following sections.

"Light green" region microvoid coalescence in the weld metal. This morphology is represented by a light green color — Fig. 9A to C. Figure 10 shows this morphology at a higher magnification of the as-welded sample — samples 640˚C/6 h and 660˚C/10 h. The morphology was classic ductile, microvoid coalescence (MVC). All these represented fracture through the weld metal as indicated by the high Ni content. This fracture surface was formed due to overload at the later stage of the cracking, rather than at the initiation stage of the cracking. Hydrogen did not assist the fracture propagation through the austenitic nickel-based alloy because the level of hydrogen present was too low to promote HAC.

In the as-welded condition, the "light green" fracture morphology covered most of the total fracture surface (> 50%) because the as-welded weld metal had a lower hardness/strength than the CGHAZ or even the base metal. As the HJP increased, the area of "light green" fracture decreased. The increasing HJP promoted precipitation hardening in the Alloy 625 weld metal, which reduced, or eliminated, overload failure in the weld metal.

"Purple" region quasi-cleavage in the CGHAZ. The morphology represented by purple is present in the as-welded sample (Fig. 9A) — samples 660˚C/10 h (Fig. 9C), 660˚C/20 h (Fig. 9D), and 660˚C/50 h (Fig. 9E). Higher magnification fractographs of these samples are shown in Fig. 11. They exhibited typically quasi-cleavage, brittle fracture surfaces with relatively low fracture energy. The fracture surfaces were relatively flat with clear evidence of quasi-cleavage.

Figure 11D shows a lath structure, suggesting a martensitic structure. These fracture paths propagated through the base metal and may have transitioned gradually to the fusion boundary surface — Fig. 11C. The EDX analysis showed that the morphologies of Fig. 11A and B exhibit Fe levels of 95 wt-%, and that the surface in Fig. 11D shows 77 wt-% Fe. It is possible that the layer of steel martensite was so thin that the EDX also detected the chemical composition of the Alloy 625 under the martensite layer. In fact, the region marked by an arrow is the fusion boundary surface — Fig. 11D.

In the as-welded condition, the fracture area indicated in "purple" is

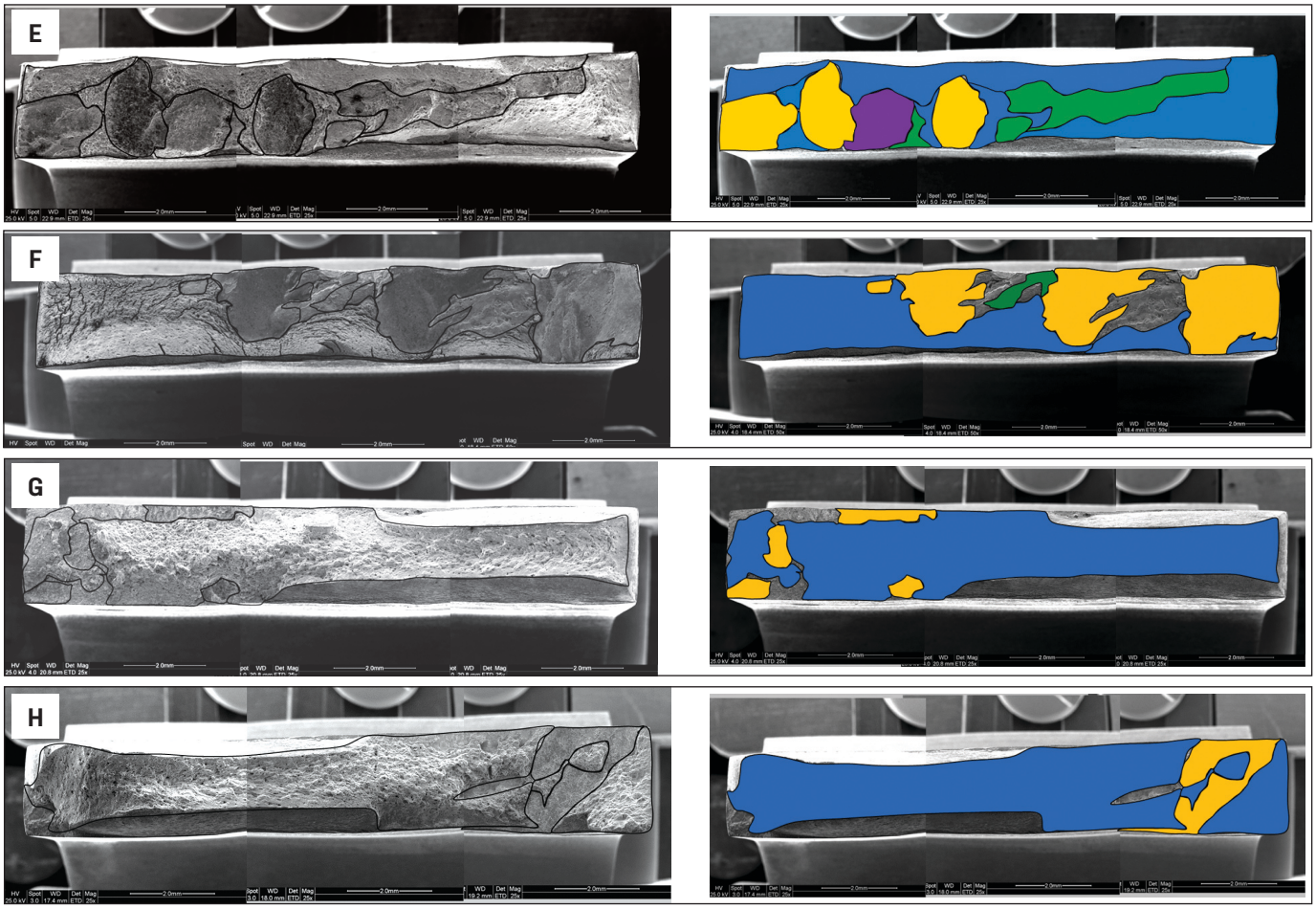

Fig. 9 (continued) — The fracture surface of different samples on the Ni-alloy 625 side and the different typical morphologies are represented by different colors: E — 660°C/50 h; F — 660°C/100 h; G — 660°C/240 h; H — 660°C/500 h. Light green = microvoid coalescence in weld metal by overload; purple = quasi-cleavage in the CGHAZ; orange = fusion boundary fracture; pink = microvoid coalescence in the base metal; dark green = quasi-cleavage, cleavage, or terrace fracture in the PGZ; blue = overload fracture in the base metal.

the largest since HAC occured preferentially in the as-welded CGHAZ containing hard martensite. The "purple" area decreased with the increasing HJP (Fig. 11A–D) due to tempering of the CGHAZ.

"Orange" region along the fusion boundary. The morphology represented by orange was observed in all the samples — Fig. 9A to H. These fracture surfaces represent the fusion boundary surface. Two types of grain boundaries can be observed on the fracture surfaces. One type is the Alloy 625 austenitic grain boundary, as indicated by yellow arrows in Fig. 12A. The second type of grain boundary is represented by the residual base metal attached to the fusion boundary surface, as indicated by the white arrows in Fig. 12A. The EDX analysis also showed that the residual metal on the fusion boundary surface had a high Fe content — Fig. 12B.

The HAC was undoubtedly responsible for this fracture morphology at the fusion boundary. At the PWHT condition 660°C/50 h and more severe conditions, the fusion boundary appeared macroscopically smooth. However, microscopically, there were precipitates present on the fusion boundary surface — Fig. 12C. Figure 12D is the base metal side of the fracture surface of Fig. 12C, PWHT 660°C/240 h. The precipitates in Fig. 12C detached from the fracture surface on the base metal side, leaving many holes with the same size on the mating surface. It is possible that the precipitates promoted the HAC because the fracture propagates along the precipitate-matrix interface, which can act as a trap for hydrogen. SEM analysis showed the precipitates did not form until PWHT at 660°C/50 h. There were only tiny precipitates on the fusion boundary surface. This can partially explain why the TTF (HAC resistance) of sample 660°C/50 h was better than samples at severer PWHT. Interestingly, the area of "orange" fracture surface increased and then decreased, corresponding to the predicted trend of TTF shown in Fig. 8.

These precipitates were plate-like in shape (Fig. 12C), with approximate dimensions of 0.1 to 0.5 µm. Precipitates of this size were seen in fracture samples from the following heat treatments: 660°C/50 h, 660°C/100 h, 660°C/240 h, and 660°C/500 h. As the HJP increased, the amount of the precipitates increased.

"Pink" region microvoid coalescence in the base metal. The mor-

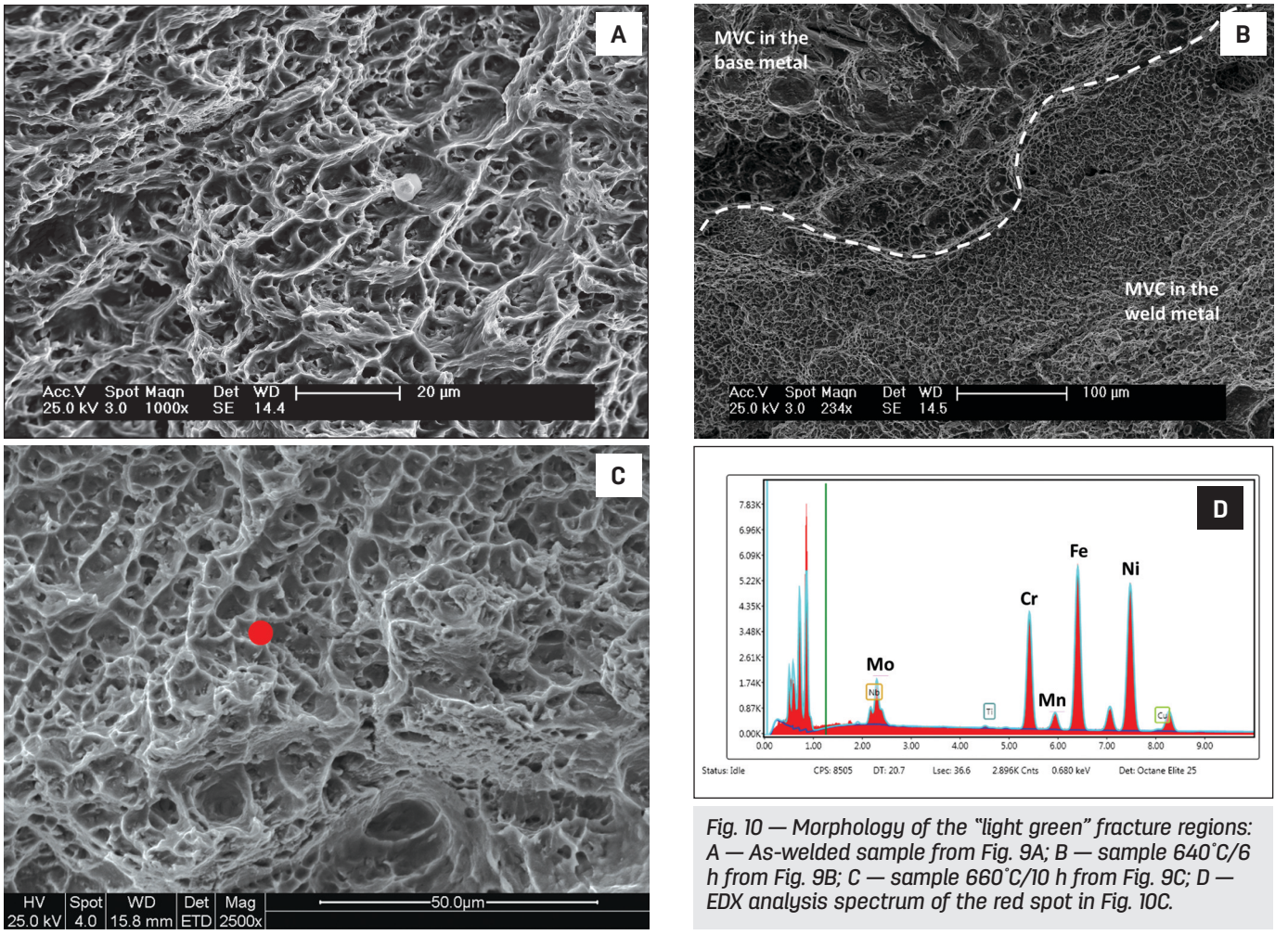

Fig. 10 — Morphology of the "light green" fracture regions: A — As-welded sample from Fig. 9A; B — sample 640˚C/6 h from Fig. 9B; C — sample 660˚C/10 h from Fig. 9C; D — EDX analysis spectrum of the red spot in Fig. 10C.

phology represented by pink regions is shown in Fig. 9B to D. Figure 13 shows a closer view of the fracture surfaces of samples 640˚C/6 h and 660˚C/10 h. This was typical ductile, microvoid coalescence similar to the light green fracture surface in Fig. 10, but it did not occur in the weld metal. The EDX analysis showed the Fe composition in this region was above 90 wt-%, and Fig. 13B shows the MVC fracture was above the fusion boundary surface, considering the fracture was on the half sample of the Alloy 625 overlay. Thus, the "pink" fracture went through the base metal, probably assisted by hydrogen. The MVC is a common HAC morphology in steel according to Beachem's theory (Refs. 18 and 21).

"Blue" region overload in the base metal. The morphology represented by blue regions appeared in all the samples — Fig. 9A to H. Only two typical samples were shown in Fig. 14 because the morphologies of the "blue" fracture surface of all the samples were similar. The EDX analysis showed that the iron content was around 95 wt-%. The morphology in the "blue" fracture was ductile rupture and occurred through the base metal due to overloading. Its morphology and formation mechanism were different from the MVC fracture shown in Fig. 13. Figure 14A shows both types of fracture morphologies and clearly indicates the contrast between coarse MVC fracture and the overload region of the fracture surface. The large depth of field in Fig. 14A shows the overloaded fracture surface was much more above the MVC fracture surface. As shown in Fig. 14B, there was a mixture of coarse and fine dimples (yellow arrow) and secondary cracks (white arrow) on the overload fracture surface.

In Fig. 9A to H, the blue area increased with the HJP. As the PWHT increases, the CGHAZ became increasingly softer. The softened base metal and HAZ became the weakest zone at a high HJP and led to overload failure after the crack propagated along the fusion boundary. This was especially the case for samples with a PWHT at 660˚C/100 h and 660˚C/240 h, where the area of the "blue" fracture surface was larger than 90%. The fracture propagated through the weak, over-tempered base metal immediately after the initiation of the fracture at the fusion boundary surface ("orange" area). The necking phenomenon can be observed in Fig. 9G and H. In addition to embrittling the fusion boundary, these two PWHT conditions reduced the strength of the base metal considerably and would not be appropriate in actual practice.

"Dark green" region quasi-cleavage in the PGZ. The morphology represented by the dark green regions appears in Fig. 9D to F. Figure 15 shows higher magnification fractographs of the samples at 660˚C/ 20 h, 660˚C/50 h, and 660˚C/100 h, respectively. The "dark green" fracture shows various morphologies: cleavage (Fig. 15A), quasi-cleavage (Fig. 15A), and/or terrace structures (Fig. 15B, C, and E), which are all typical HAC

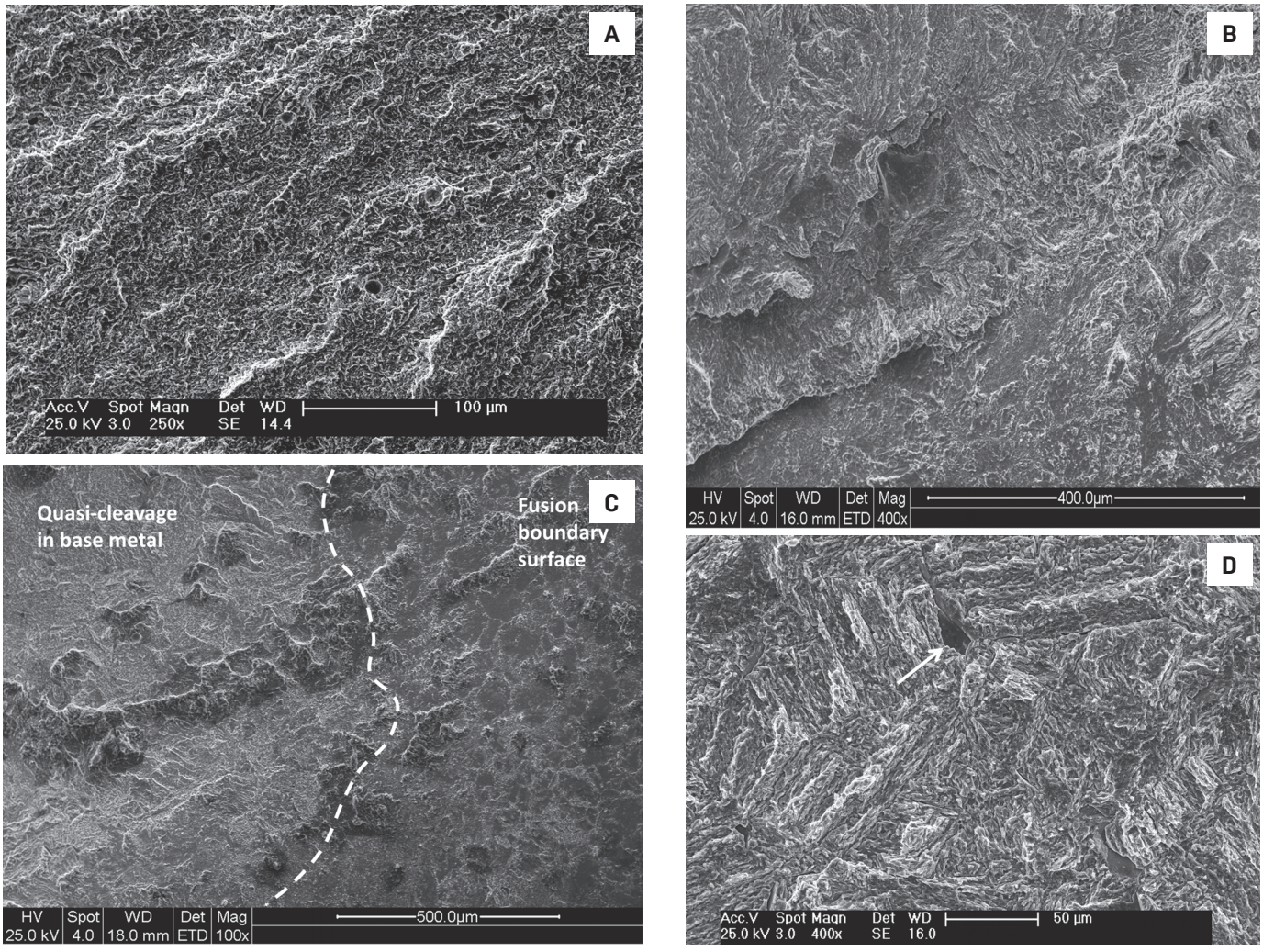

Fig. 11 — Morphology of the "purple" fracture in different PWHT conditions: A — As-welded sample from Fig. 9A; B — sample 660˚C/10 h from Fig. 9A; C — sample 660˚C/20 h from Fig. 9D; D — sample 660˚C/50 h from Fig. 9E.

morphologies. The EDX mapping demonstrated qualitatively that the terrace fracture contained mainly nickel (Alloy 625), but did not show any evidence of cellular or dendritic growth in the fusion zone. Thus, it appears that the "dark green" fracture initiated or propagated through the PGZ.

It is likely that the "dark green" regions were the initiation sites of the HAC. For samples 660˚C/20 h, 660˚C/50 h, and especially 660˚C/50 h, the "dark green" fracture was in the inner area of the entire fracture. When the HAC initiated in the "dark green" area, the cracking propagated into the overtempered base metal in all directions and produced the ductile, overloaded fracture (blue) around the HAC initiation area — Fig. 15F.

Discussion

Relationship between the Hollomon -Jaffe Parameter and HAC Susceptibility

The DHCT results confirmed the HAC susceptibility of the F22/625 overlay interface region was a strong function of the HJP as indicated by the TTF. The TTF was maximum (highest resistance) in the HJP range of 19,800 to 20,200. The optimal PWHT range based on hardness testing was the HJP from ~19,500 to 19,800, in which the HAZ hardness was reduced below the industry standard without strong hardening (embrittlement) of the planar growth zone at the weld interface — Figs. 7, 8, and 16. The PWHT range inferred from the hardness testing did not overlap the DHCT results, probably because the HAC susceptibility was determined not only by the hardness of the susceptible microstructure, but also by the location of the susceptible microstructure relative to the surface of the sample. While hardness is a good indicator of TTF in the DHCT, it is not the only factor controlling the TTF. The PGZ and CGHAZ with the same hardness may have different susceptibilities to HAC due to differences in both composition and microstructure. The area of the CGHAZ is much greater than the narrow PGZ adjacent to the fusion boundary, and this may influence crack initiation.

The hardness of three regions and the TTF was plotted together in Fig. 16. Based on these results, it appears that a tempering "sweet spot" exists in an HJP

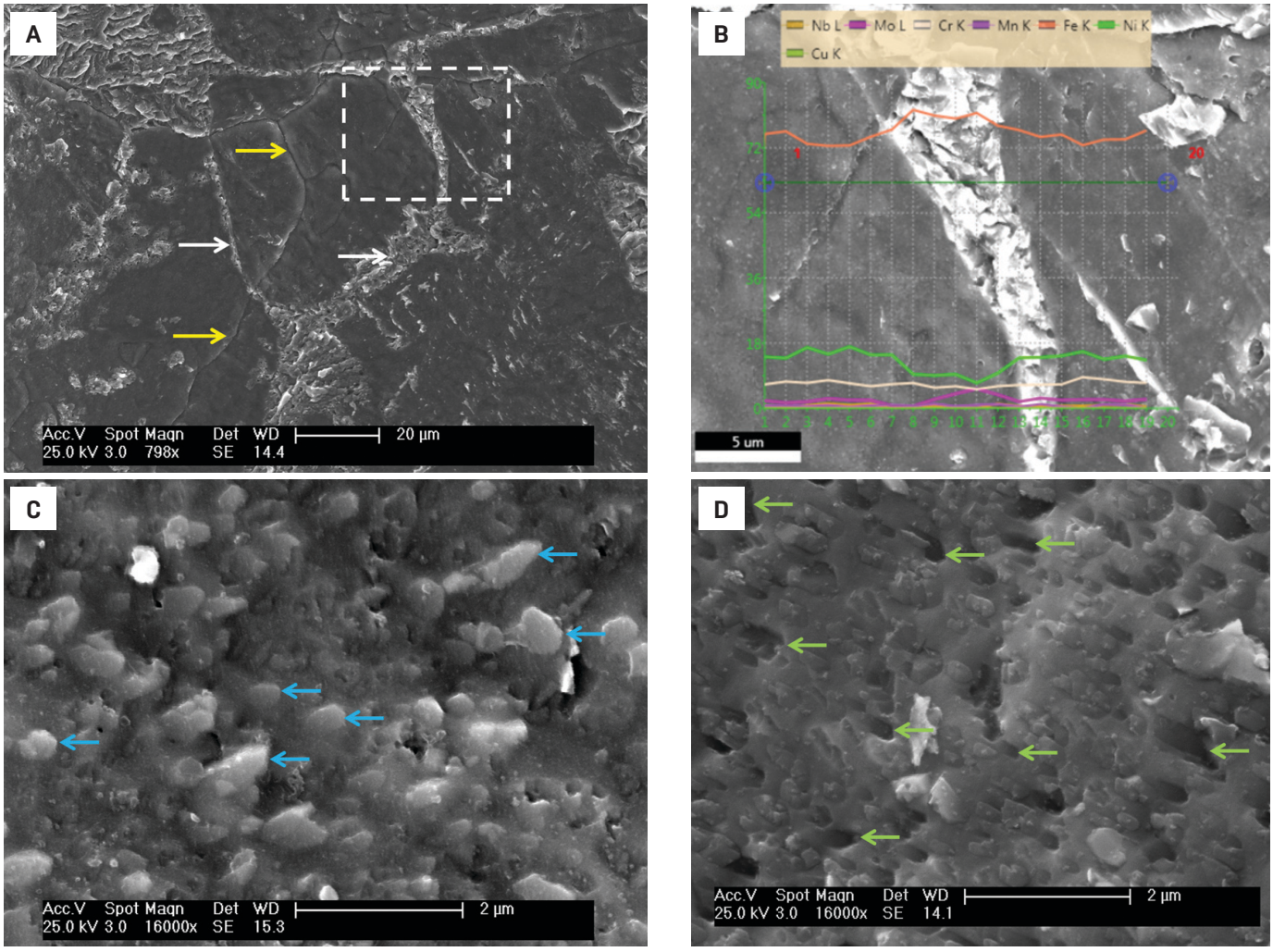

Fig. 12 — Typical morphology of the "orange" fracture in the selected PWHT conditions: A — Sample 660°C/10 h from Fig. 9C. White arrows show the CGHAZ grain boundaries, and yellow arrows show the PGZ boundaries; B — EDX line scan across the residual metal in the framed area in Fig. 12A; C — precipitates indicated by the blue arrows on the fracture surface of the Alloy 625 side of sample 660°C/240 h; D — "holes" indicated by the green arrows on the fracture surface of the base metal side of sample 660°C/240 h.

range from 19,800 to 20,200. For example, PWHT at 660°C/20 h resulted in a CGHAZ hardness below 250 VHN as well as a PGZ and weld metal hardness of ~300 VHN. Multiple DHCT tests of samples subjected to this heat treatment resulted in near-maximum values of TTF, indicating good resistance to HAC. At lower values of HJP, TTF dropped off due to high hardness in the CGHAZ. While at higher values (> 20,200 HJP), TTF decreased due to embrittlement of the PGZ or fusion boundary by carbon buildup and carbides precipitation, which will be further discussed in the next section.

The cleavage and quasi-cleavage ("dark green") fracture morphology (Fig. 9D and E) in the inner area of the whole fracture surface is surrounded by a "blue" fracture area on the sample within the "sweet spot" (660°C/20 h and 660°C/50 h). It is presumed that this represents the HAC initiation site based on the fracture surface features. The initiation sites for these two samples were both in the PGZ. If HAC initiated from the sample interior rather than from the surface, longer failure times would be expected due to the rate-limiting time for hydrogen to diffuse into the inner area of the sample. Thus, the HAC resistance of the PWHT 660°C/50 h was optimal based on the highest TTF and acceptable hardness in the CGHAZ.

For the 660°C/20 h condition, there was a similar fracture initiation area (dark green area in Fig. 9D), and its TTF was also high. This then defined the optimum HJP range of 19,800 to 20,200. Although the PWHT times (20 and 50 h) used in this study to identify an optimal PWHT were excessive from a practical standpoint, slightly higher PWHT temperatures (e.g., 680°C) could be used to achieve the same HJP range at shorter times. Since 680°C is below the A_{c1} of the F22 steel (Ref. 22), this PWHT temperature was a possible option to reduce the overall heat treatment time. The effect of longer PWHT times and/or higher HJP values on the softening of the base metal should also be considered.

Fractography

Six fracture morphologies were observed on the failed sample surfaces as a function of tempering conditions, and they were color-coded to allow easy comparison. The "light green" and "blue" fracture surfaces were

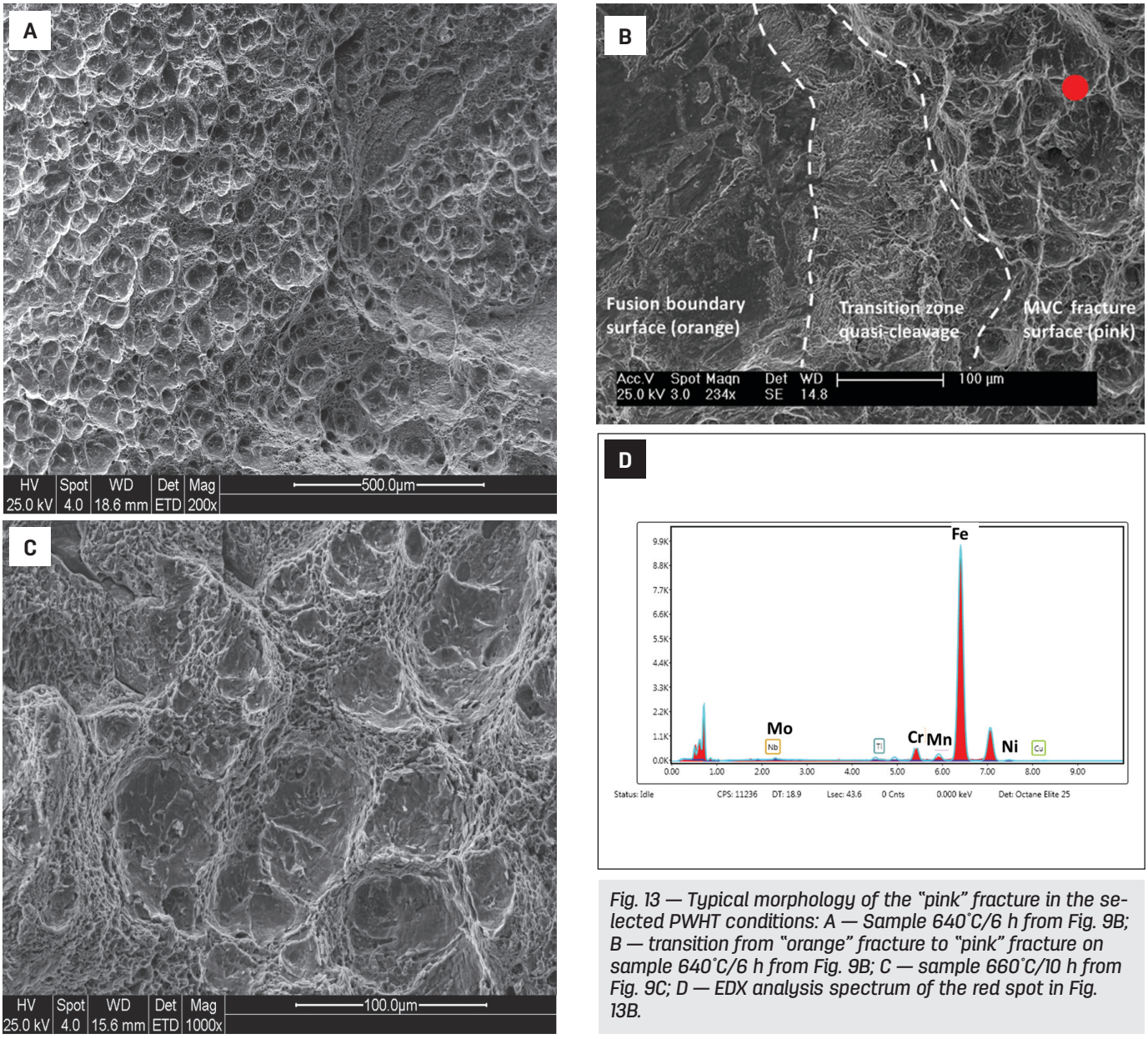

Fig. 13 — Typical morphology of the "pink" fracture in the selected PWHT conditions: A — Sample 640°C/6 h from Fig. 9B; B — transition from "orange" fracture to "pink" fracture on sample 640°C/6 h from Fig. 9B; C — sample 660°C/10 h from Fig. 9C; D — EDX analysis spectrum of the red spot in Fig. 13B.

formed due to overload failure through the Alloy 625 weld metal and F22 base metal, respectively, and do not represent failure by HAC. As described in Beachem's theory, depending on the combination of hydrogen concentration and the stress intensity factor at the crack tip, the typical HAC fracture surface morphologies include intergranular (IG), quasi-cleavage (QC), and microvoid coalescence (MVC) (Refs. 18 and 21). The latter two are also called transgranular fracture. The IG morphology is the fracture that propagates along the prior austenite grain boundaries (Ref. 23).

The QC morphology was found in "dark green" and "purple" fracture regions, and MVC morphology was represented by "pink" fracture. Thus, the "dark green," "purple," and "pink" fractures represented forms of HAC according to Beachem's theory (Ref. 21). Pure IG fracture was not observed, but the "orange" fracture at the fusion boundary surface approximated the IG morphology, and thus is thought to be HAC. Other evidence of HAC is related to precipitates that formed in heavily tempered samples because they seemed to promote the HAC due to the separation of the precipitates from the matrix on the fracture surface, as shown by the fracture morphology of sample 660°C/240 h in Fig. 12C. The HAC fracture morphologies were also studied on a F22/625 sample tempered at 650°C/100 h (HJP = 20,306) by Dodge (Ref. 6). He found fusiform M_7C_3 in the scale of 100 nm in the PGZ, but did not report the presence of precipitates found in our work, as described previously. This can possibly be attributed to the difference in the F22 composition, welding parameters, and/or tempering procedure.

The "purple" and "dark green" regions are HAC initiation sites. For the as-welded sample (Fig. 9A), the HAC initiated in the CGHAZ with a high hardness and a martensitic microstructure. As the HJP increased, the HAC initiation location moved from the CGHAZ to the fusion boundary, as summarized in Table 5. The maximum HJP from Dodge's work (Ref. 6) was 20,306 (650°C/100 h). In

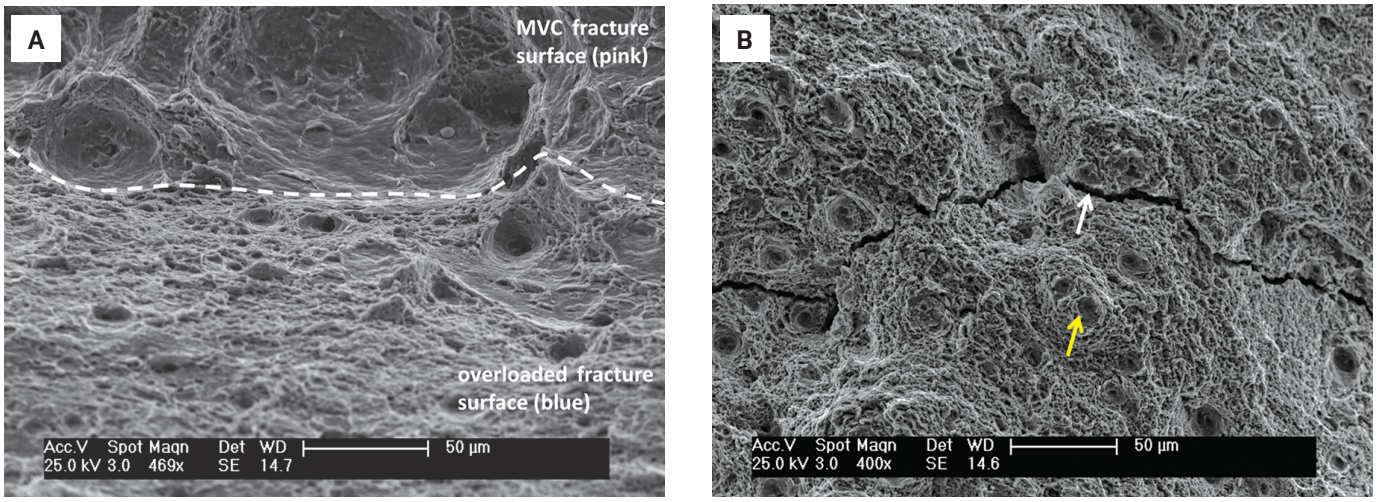

Fig. 14 — Typical morphology of the "blue" fracture regions in the selected PWHT conditions: A — Sample 640˚C/6 h from Fig. 9B shows the contrast between the "pink" and "blue" fractures; B — sample 660˚C/50 h from Fig. 9E. The white arrow shows a secondary crack in the CGHAZ. The yellow arrow shows a large dimple due to precipitates.

this PWHT condition, he found the HAC initiated and propagated mainly through the PGZ, where the precipitation of M_7C_3 promoted the HAC.

In this work, larger HJPs were also studied: 20,526 (660˚C/100 h), 20,881 (660˚C/240 h), and 21,178 (660˚C/500 h). Precipitates were found at the fusion boundary in the three PWHT conditions, as indicated by the white arrows in Fig. 12C. The precipitates promoted the HAC and probably made the fusion boundary ("orange" region) become more susceptible to HAC than the PGZ. Thus, the fusion boundary became the HAC initiation location again.

Observations Regarding the Delayed Hydrogen Cracking Test

In the hydrogen-charging circuit of the DHCT system, the sample was the cathode, and the cathodic reaction at the sample surface was the following (Refs. 15 and 24):

$$2H^+ + 2e^- \rightarrow H_2 \text{ or } 2H \qquad (2)$$

The platinum wire was the anode, but the anodic reaction had not been reported by previous researchers. It is proposed to be the following, but needs further confirmation:

$$H_2O \rightarrow \tfrac{1}{2}O_2 + 2H^+ + 2e^- \qquad (3)$$

Unlike the precharged bend test and slow-strain rate test (Refs. 12 and 14), the DHCT is a recently developed test that applies constant loading while the sample is charged. This simulates the scenario of cathodic protection that is used in practice for offshore platforms. However, the DHCT is an accelerated HAC test with a lower pH-charging solution and stronger charging current. Hydrogen charging started immediately after the sample was loaded. The hydrogen charging time of each sample equaled its TTF and differed from other samples. Thus, the amount of charged hydrogen in one sample was different from the other, but the amount must be adequate for HAC as long as the sample failed in the DHCT.

There are only four parameters that control the DHCT, including charging-current density, hydrogen-charging solution pH, the amount of hydrogen recombination poison, and sample load (stress). For the data reported here, all of these variables were kept constant. Thus, the only experimental variable was the PWHT condition as quantified by the HJP. The hydrogen recombination poison was sodium thiosulfate ($Na_2S_2O_3$), which is not as hazardous as As_2O_3, but less stable in the sulfuric acid solution. It reacts with sulfuric acid to produce sulfur (S) and sulfur dioxide (SO_2), as shown by Ref. 25:

$$H_2SO_4 + Na_2S_2O_3 \rightarrow H_2O + Na_2SO_4 + S\downarrow + SO_2\uparrow \qquad (4)$$

Previous researchers (Refs. 13–15) did not address this reaction. The reactant SO_2 is the actual hydrogen recombination poison, which prevents the combination of hydrogen atoms to form hydrogen gas and promotes the introduction of atomic hydrogen into the sample, but the mechanism needs further investigation. SO_2 is in gas form at ambient temperature and pressure, and it may release partially from the charging solution as time goes by. Thus, a new charging solution was used for each sample. The test should start after the same period of time for all samples to ensure thorough reaction between H_2SO_4 and $Na_2S_2O_3$, and equal testing conditions. After trial and error testing, a period of 24 h was used.

Although the general trend of the TTF with the HJP (Fig. 6) is quite clear and consistent with tempering effects on microstructure, the TTF exhibited some scatter, especially for PWHT 660˚C/50 h, 660˚C/240 h, and 660˚C/500 h. There are several reasons for this. First, the PGZ microstructure of the F22/625 sample periodically varied along the fusion boundary, especially the width of the PGZ and the presence of a "swirl structure" (Refs. 5–7). When considering duplicate samples with the same PWHT condition, one sample may have a susceptible feature such as a swirl on the edge, and another may not. The sample with the susceptible microstructure on the edge had a shorter TTF because it took less time for the hydrogen to diffuse into the susceptible microstructure.

Second, the sample gauge section was manually ground with a 600-grit abrasive to remove oxidation, which can potentially inhibit the introduction of hydrogen atoms. Slight differ-

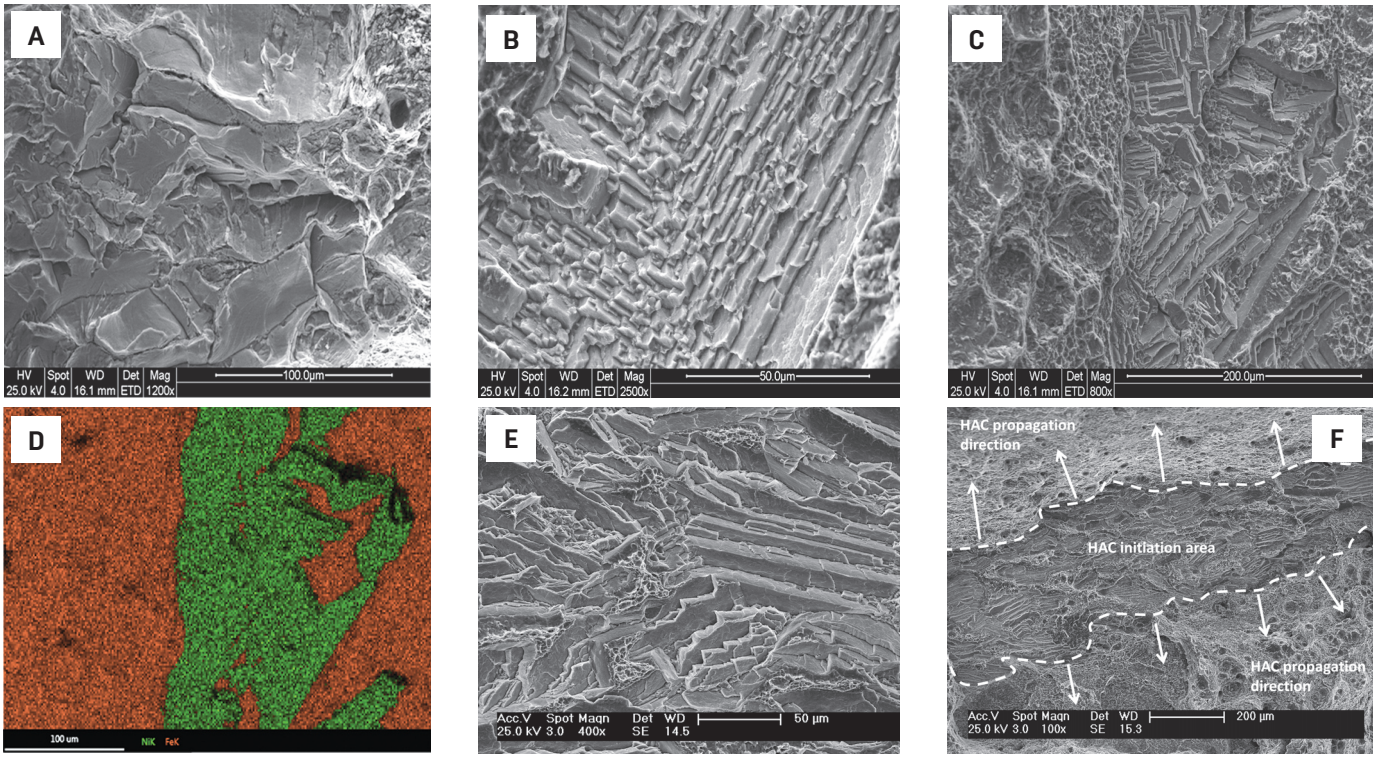

Fig. 15 — Typical morphology of the "dark green" fracture in the selected PWHT conditions: A — Cleavage and quasi-cleavage fracture surface of sample 660°C/20 h from Fig. 9D; B — terrace fracture surface of sample 660°C/20 h from Fig. 9D; C — terrace fracture surface surrounded by a more ductile fracture surface of sample 660°C/20 h from Fig. 9D; D — the EDX map of Fig. 15C; E — terrace fracture surface of sample 660°C/50 h from Fig. 9E; F — HAC initiation area surrounded by HAC propagation area, with propagation directions shown.

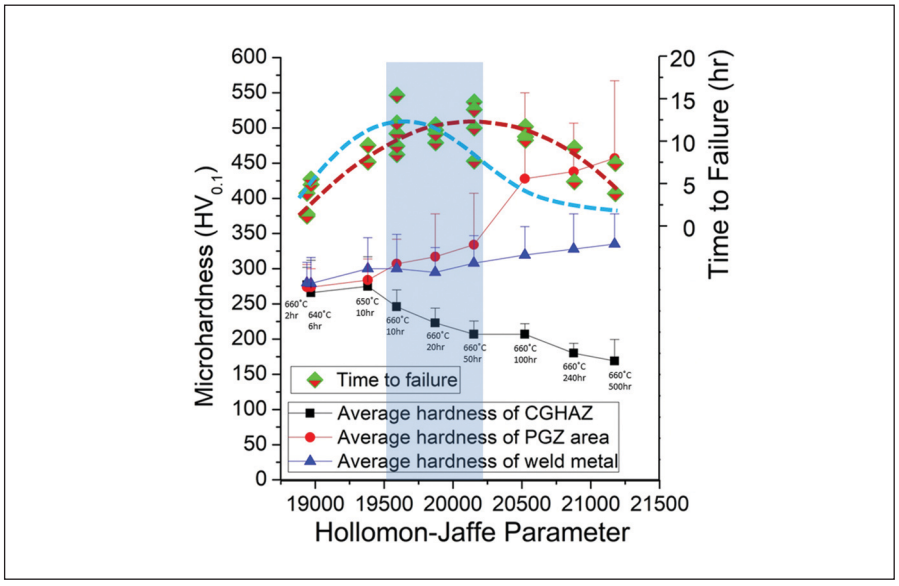

Fig. 16 — Comparison of the TTF trend (blue dashed curve) inferred from hardness results and the TTF trend from the DHCT results (red dashed curve).

ences in surface conditions can also affect hydrogen uptake.

Third, the presence of SO_2 may create variability in the charging solution. A method needs to be developed to measure the content of dissolved SO_2 in solution and to ensure all the charging solutions have equal content of dissolved SO_2.

Finally, the influence of load (stress) is extremely important. The load must be such that failure occurs within reasonable experimental time. If the load is too large, the TTF will be too short, and differences due to PWHT may be hard to determine. If the load is too low, testing times can be excessive or failure will not occur. The selection of the constant load (stress) in this study ensured that failure occurred in a reasonable experimental timeframe while reflecting the metallurgical condition of the F22/625 interface.

Conclusions

1) The delayed hydrogen cracking test (DHCT) confirmed HAC resistance (indicated by time-to-failure) of the F22/625 overlay interface is a strong function of the Hollomon-Jaffe parameter (HJP).

2) Based on the DHCT results and hardness testing, a PWHT "sweet spot" appears to exist in the HJP range of ~19,500 to 20,200, which includes PWHT 660°C/10 h, 660°C/20 h, and 660°C/50 h.

3) The PWHT of 660°C/10 h (HJP = 19,593) is a probable optimal condi-

tion, since the average CGHAZ hardness is below 250 VHN with little hardening (embrittlement) of the planar growth zone at the weld interface. Also, this PWHT is close to the peak time-to-failure in the DHCT.

4) Six typical morphologies were found on the fracture surfaces of the tempered samples. Two fracture morphologies resulted from overloading, and the other four fracture morphologies were associated with HAC.

5) Precipitation was found on the fracture along the fusion boundary surface for the tempering conditions 660°C/100 h, 660°C/240 h, and 660°C/500 h. These precipitates appear to be initiation sites for HAC.

6) The DHCT on F22/625 dissimilar weld metal samples confirmed the effectiveness and reliability of this HAC testing method, but the test method could be improved if the dissolved SO_2 content in the solution was measured.

Acknowledgments

This work was originally supported by Cameron International and Acute Technological Services through the NSF I/UCRC for Manufacturing & Materials Joining Innovation Center (MA²JIC). Thanks to Dean Hannam and Nash Ubale from Schlumberger (formerly Cameron International) for arranging the procurement of the F22 materials as well as providing advice and guidance throughout the project. Also, thanks to Tim Thompson for providing the Alloy 625 welding wire and conducting the F22/625 overlay cladding.

References

1. International Organization for Standardization. ISO 15156-2:2009, *Petroleum and Natural Gas Industries — Materials for Use in H_2S-Containing Environments in Oil and Gas Production — Part 2: Cracking-Resistant Carbon and Low Alloy Steels and the Use of Cast Irons*.

2. Olden, V., Kvaale, P. E., Simense, P. A., Aaldstedt, S., and Sloberg, J. K. 2003. The effect of PWHT on the materials properties and microstructure in Inconel 625 and Inconel 725 buttered joints. *The 22nd International Conference on Offshore Mechanics & Arctic Engineering*, p. 7. Cancun, Mexico.

3. Beaugrand, V. C., Smith, L. S., and Gittos, M. F. 2009. Subsea dissimilar joints: Failure mechanisms and opportunities for mitigation. *Corrosion*: 14.

4. Gittos, M. F., and Gooch, T. G. 1992. The interface below stainless steel and nickel-alloy claddings. *Welding Journal* 71(12): 461-s to 472-s.

5. Dai, T., and Lippold, J. C. 2017. Tempering behavior of the fusion boundary region of Alloy 625 weld overlay on 2.25Cr-1Mo steel. *Welding Journal* 96(12): 467-s to 480-s.

6. Dodge, M. F. 2014. The effect of heat treatment on the embrittlement of dissimilar welded joints. Master's thesis. Univeristy of Leicester, Leicester, UK.

7. Fenske, J. A. 2010. Microstructure and hydrogen induced failure mechanisms in iron-nickel weldments. PhD dissertation. University of Illinois at Urbana-Champaign, Urbana, Ill.

8. Luppo, M. I., and Ovejero-Garcia, J. 1991. The influence of microstructure on the trapping and diffusion of hydrogen in a low carbon steel. *Corrosion Science* 32(10): 1125–1136.

9. Nagao, A., Smith, C. D., Dadfarnia, M., Sofronis, P., and Robertson, I. M. 2012. The role of hydrogen in hydrogen embrittlement fracture of lath martensitic steel. *Acta Materialia* 60(13–14): 5182–5189.

10. Wang, M., Akiyama, E., and Tsuzaki, K. 2007. Effect of hydrogen on the fracture behavior of high strength steel during slow strain rate test. *Corrosion Science* 49(11): 4081–4097.

11. Symons, D. M. 1997. Hydrogen embrittlement of Ni-Cr-Fe alloys. *Metallurgical and Materials Transactions A* 28(3): 655–663.

12. Symons, D. M. 1998. The effect of carbide precipitation on the hydrogen-enhanced fracture behavior of Alloy 690. *Metallurgical and Materials Transactions A* 29(4): 1265–1277.

13. Alexandrov, B., Shi, S., Rodelas, J. M., and Lippold, J. C. 2012. A new test for evaluation of susceptibility to hydrogen assisted cracking in dissimilar metal welds. *NACE Corrosion Conference & Expo*, Houston, Tex.

14. Steiner, J. M. 2014. Phase transformation behavior and hydrogen cracking susceptibility in Grade T23 and T24 steel welds. Master's thesis. The Ohio State University, Columbus, Ohio.

15. Bourgeois, D. 2015. Hydrogen assisted crack in dissimilar metal welds for subsea service under cathodic protection. PhD dissertation. The Ohio State University, Columbus, Ohio.

16. Foroulis, Z. A. 1981. The influence of promoter elements in acidic sulfate solutions on hydrogen absorption in titanium. *Journal of the Electrochemical Society* 128(1): 219–221.

17. Bolzoni, F., Fassina, P., Fumagalli, G., Lazzari, L., and Re, G. 2010. Hydrogen charging of carbon and low alloy steel by electrochemical methods. *EuroCorr Conference,* Moskva, Moscow.

18. Yue, X. 2013. Evaluation of heat-affected zone hydrogen-induced cracking in high-strength steels. PhD dissertation. The Ohio State University, Columbus, Ohio.

19. Fenske, J. A., Robertson, I. M., Ayer, R., Husle, M., Lillig, D., and Newbury, B. 2012. Microstructure and hydrogen-induced failure mechanisms in Fe and Ni alloy weldments. *Metallurgical and Materials Transactions A* 43(9): 3011–3022.

20. Hollomon, J., and Jaffe, L. 1945. Time-temperature relations in tempering steel. *Metal Technology* 12: 223–249.

21. Beachem, C. 1972. A new model for hydrogen-assisted cracking (hydrogen "embrittlement"). *Metallurgical and Materials Transactions B* 3(2): 441–455.

22. Bhadeshia, H. K. D. H. 2001. *Bainite in Steels: Transformations, Microstructure and Properties*. London: Institute of Materials.

23. Lippod, J. C. 2014. *Welding Metallurgy and Weldability*. Hoboken, N.J.: John Wiley & Sons Inc.

24. Cheng, Y. F., and Niu, L. 2007. Mechanism for hydrogen evolution reaction on pipeline steel in near-neutral pH solution. *Electrochemistry Communications* 9(4): 558–562.

25. Department of Chemistry, Moscow State University: *chem.msu.su/eng/teaching/Kinetics-online/experiments.html*.

26. Berkowitz, B. J., and Heubaum, F. H. 1984. The role of hydrogen in sulfide stress cracking of low alloy steels. *Corrosion* 40(5): 240–245.

27. NACE International. TM0177-2005, *Laboratory Testing of Metals for Resistance to Sulfide Stress Cracking and Stress Corrosion Cracking in H2S Environment*.

TAO DAI (daitao11@gmail) *and JOHN C. LIPPOLD are with the Welding Engineering Program at The Ohio State University, Columbus, Ohio.*